

# Inverse $k$ -visibility for RSSI-based Indoor Geometric Mapping

Junseo Kim, *Member, IEEE*, Matthew Lisondra, *Member, IEEE*, Yeganeh Bahoo, and Sajad Saeedi, *Member, IEEE*

**Abstract**—In recent years, the increased availability of WiFi in indoor environments has gained an interest in the robotics community to leverage WiFi signals for enhancing indoor SLAM (Simultaneous Localization and Mapping) systems. SLAM technology is widely used, especially for the navigation and control of autonomous robots. This paper discusses various works in developing WiFi-based localization and challenges in achieving high-accuracy geometric maps. This paper introduces the concept of *inverse  $k$ -visibility* developed from the  $k$ -visibility algorithm to identify the free space in an unknown environment for planning, navigation, and obstacle avoidance. Comprehensive experiments, including those utilizing single and multiple RSSI signals, were conducted in both simulated and real-world environments to demonstrate the robustness of the proposed algorithm. Additionally, a detailed analysis comparing the resulting maps with ground-truth Lidar-based maps is provided to highlight the algorithm’s accuracy and reliability.

## I. INTRODUCTION

Simultaneous localization and mapping (SLAM) is an essential process, involving self-localizing and construction of a map of the environment, especially important for self-navigating autonomous robots. Current state-of-the-art approaches rely heavily on sensors like cameras, IMUs (Inertial Measurement Units), laser range finders, and ultrasound. These sensors provide data that is used to generate accurate estimates of the environment map. However, cameras, laser range finders, and ultrasound sensors can be obstructed, corrupted by noise, or cause privacy concerns. Therefore, alternative approaches are essential when these exteroceptive sensors are unreliable or insufficient. Developing robust methods that can compensate for these limitations is critical to improving overall performance and ensuring accurate environment mapping in diverse and challenging conditions.

As WiFi networks occupy many indoor and public spaces, the use-case of information extruding from WiFi systems is a promising alternative for achieving SLAM accuracy. Such information is known as received signal strength indicator (RSSI) data, protruding outward from WiFi emitters. This method is particularly advantageous in situations where traditional sensors such as cameras, lasers, and ultrasound may be

inadequate, such as in environments with privacy concerns or poor lighting conditions [1]. The recent progress in this domain, such as *WiFiSLAM*[2], has predominantly concentrated on WiFi-based localization and the potential estimation of WiFi router positions, without generating a geometric map of the environment, needed for many robotic applications. There have been works relying on crowdsourcing [3], showing that it is possible to generate an environment map using WiFi data. However, these methods often face challenges such as limited accuracy due to signal interference, variability in signal strength, and the need for extensive data from multiple users for reliable results. Additionally, processing of the map with primarily RSSI information in the algorithms of many works, shows that it fluctuates unstably, being unreliable, particularly in environments that are dynamically changing [4]. Thus, it is clear that there exists a gap in the development of a way in which to leverage a WiFi-based mapping technique, from geometric constraints alone. The main problem arises in acquiring, from the WiFi data, an accurate geometric shape of the true mapped environment.

This paper<sup>1</sup> presents a novel technique capable of generating geometric maps from WiFi signals. The method utilizes developments in computational geometry, namely the  *$k$ -visibility* algorithm [6]. We extend the  *$k$ -visibility* by presenting the concept of *inverse  $k$ -visibility*. This novel concept is then utilized to develop a geometric map of an unknown environment from WiFi signals, coined Structure from WiFi (SfW).

Knowing accurately the mapped free space is imperative for the control of many autonomous systems, which need to know how to plan paths, making sure not to collide with occupied and obstacle spaces. The contributions of our work are:<sup>2</sup> 1) A novel algorithm that is capable of generating geometric maps using WiFi signals received from multiple routers, 2) benchmarking the WiFi-generated maps with Lidar-generated maps by comparing the area, number of data points,  $k$ -value prediction True/False setting,  $k$ -value accuracy percentage, IOU and MSE scores, and 3) evaluation on real-world collected from indoor spaces.

The rest of this work is organized as follows: Sec. II presents an overview of recent approaches to WiFiSLAM and challenges faced in applications. Sec. III describes the background of  $k$ -visibility algorithm. Sec. IV proposes the inverse  $k$ -visibility algorithm. Sec. V extends the inverse  $k$ -visibility algorithm to real-world experiments utilizing

<sup>1</sup>This paper is partly based on our earlier paper [5], extended with multiple routers, metric evaluations, and more experiments.

<sup>2</sup><https://sites.google.com/view/structure-from-wifi/home>

Manuscript received August 8, 2024; accepted MM DD, YEAR. Date of publication MM DD, YEAR; date of current version MM DD, YEAR. We acknowledge the support of the Natural Sciences and Engineering Research Council of Canada (NSERC). The associate editor coordinating the review of this article and approving it for publication was Prof. TBD. (Corresponding author: Junseo Kim.)

Junseo Kim, Matthew Lisondra, and Sajad Saeedi are with the Mechanical, Industrial, and Mechatronics Engineering Department, Toronto Metropolitan University, Toronto, ON (e-mail: junseo.kim, matthew.lisondra, s.saeedi@torontomu.ca).

Yeganeh Bahoo is with the Computer Science Department, Toronto Metropolitan University, Toronto, ON (e-mail: bahoo@torontomu.ca).

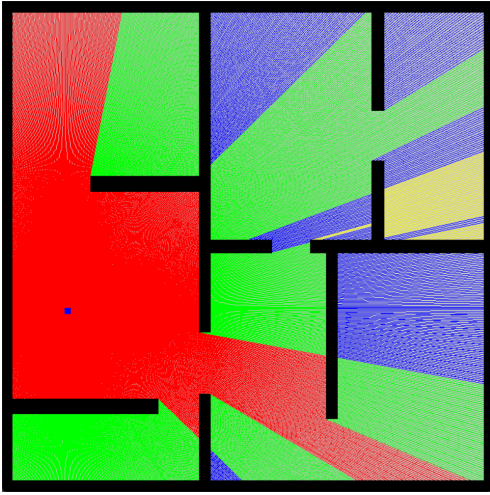


Fig. 1. The concept of  $k$ -visibility is demonstrated where different  $k$ -values are shown:  $k = 0$  (red),  $k = 1$  (green),  $k = 2$  (blue) and  $k = 3$  (yellow). Based on a straight-line measure from a reference point such as a router (shown in dark blue) to a desired location,  $k$ -visibility is a metric on how many times traverses through a wall/obstacle.

sparse information. Sec. VI presents the experimental results. Finally, Sec. VI-D discusses future works, limitations, and concludes the paper.

## II. LITERATURE REVIEW

The following section reviews recent progress in WiFi-only SLAM algorithm and wireless-based mapping technologies, pointing out the challenges encountered in generating a precise environment map from signal-strength data.

WiFi-based localization techniques have seen extensive adoption in recent years. Ferris *et al.* [2] succeeded in localization by converting high-dimensional signal strength data into a two-dimensional latent space and resolving SLAM using Gaussian Process Latent Variable Modeling (GP-LVM). This work was followed by other studies, including, [7], [8]. Graph-based algorithms for SLAM have also been explored, as in [4], [9]–[11]. Enhancements in WiFi observation models have shown potential for high-accuracy mapping, as described in the research by [1], [12]. Both learning and non-learning methods have their advantages and disadvantages, depending on the robotic system. We will first address learning-based WiFi map construction approaches (See Sec. II-A), and go through non-learning, geometric WiFi-map methods (See Sec. II-B)

### A. Learning-Based WiFi Approaches

The prominence of learning-based WiFi map construction has alleviated many issues with conventional geometric methods, but with the disadvantage of increased computational need in its pre- and post-processing steps [13], [14]. Zou *et al.* [15] introduced WiGAN, a generative adversarial network (GPR-GAN) for constructing detailed indoor radio maps using Gaussian process regression (GPR) with received signal strengths (RSS). Other notable works include [16], [17], [18], and [19]. Zhang *et al.* [20] proposed a deep fuzzy forest to address the limitations of decision trees and deep neural networks in end-to-end training for WiFi-based indoor

robot positioning. Additionally, Ayinla *et al.* [21] developed SALLoc, a WiFi fingerprinting indoor localization scheme using Stacked Autoencoder (SAE) and Attention-based Long Short-Term Memory (ALSTM), which demonstrated high accuracy and robustness in large-scale indoor environments. Wang *et al.* [22] introduced MapLoc, an LSTM-based indoor localization system that uses uncertainty maps created from magnetic field readings and WiFi RSS, showing superior performance in location prediction. Park *et al.* [23] reviewed various machine learning techniques for WiFi-based indoor positioning, emphasizing their potential to enhance accuracy and scalability. Turgut and Gorgulu Kakisim [24] proposed a hybrid deep learning architecture combining LSTM and CNN for WiFi-based indoor localization, achieving higher accuracy than baseline methods.

### B. Non-Learning-Based WiFi Approaches

The alternative to Deep learning (DL) and Machine learning (ML) modelling deals with non-learning methods. Several studies have leveraged the sensors integrated into smartphones to infer indoor floor plans through a crowdsensing approach [3]. Research in this area often utilizes inertial sensors alongside WiFi signal strength data, both of which are common in commercial smartphones. Key papers include [25]–[32]. The main limitation of these studies is that they only produce “traversable maps”, identifying navigable areas while leaving occupied zones uncharted. Additionally, these works rely on crowdsourced or public data, which may not always be accessible, thereby restricting their applicability.

In a different approach, Gonzalez-Ruiz and Mostofi [33] introduced a method to generate a non-invasive occupancy grid map using wireless measurements and directional antennas. Their framework employed a coordinated robot setup to create a 2D map of an environment by collecting data through walls and other obstacles. Similar techniques have been applied in Ultra Wide-band (UWB) SLAM studies, utilizing UWB signal path propagation models with directional antennas to achieve similar goals [34], [35].

Further, non-learning methods that do not rely on model predictions, such as Tong *et al.* [36], achieve decimeter-level localization accuracy by segmenting Wi-Fi access points (APs) into groups. These methods generate local maps from the APs and then merge them to create a comprehensive global Wi-Fi map. Ninh *et al.* [37] proposed a random statistical method for WiFi fingerprinting, achieving a maximum positioning error of less than 0.75 meters. Shi *et al.* [38] introduced a training-free indoor localization approach using WiFi round-trip phase and factor graph optimization, achieving a mean absolute error (MAE) of 0.26 meters. Estrada *et al.* [39] developed an indoor positioning system using OpenWRT, achieving an average margin error of 2.43 meters. Tao and Zhao [40] presented algorithms leveraging extreme values for AP selection and positioning, demonstrating improved accuracy. Sulaiman *et al.* [41] explored radio map generation methods to enhance RSSI-based indoor positioning, achieving approximately 0.45 meters accuracy. Azaddel *et al.* [42] proposed SPOTTER, a WiFi and

BLE fusion method based on particle filtering, showing a 35% improvement in accuracy. Tao et al. [43] introduced CBWF, a lightweight WiFi fingerprinting system achieving an average localization accuracy of 2.95 meters. Tang et al. [44] combined WiFi and vision for map construction and maintenance, enhancing accuracy and stability. Finally, Jurdi et al. [45] presented WhereArtThou, a WiFi-RTT-based indoor positioning system, achieving 90th percentile distance errors of 1.65 meters, suitable for commercial deployment.

### III. BACKGROUND: $k$ -VISIBILITY

The concept of  $k$ -visibility offers a unique perspective on WiFi systems and will be used throughout our algorithms. This concept was initially introduced as the *modem illumination problem* [46], [47].  $k$ -visibility investigates the extent of area that can be observable from the router points at the vertices of a polygon. This concept is an extension of the basic *visibility problem*, which focuses on determining the region that a single point within a polygon can see [6].

In a simple polygon  $P$ , two points  $p$  and  $q$  are considered to be mutually visible if the straight line connecting them does not intersect the exterior of  $P$  [6]. The visibility idea came from the Art Gallery Problem posed by Victor Klee in 1973 [48], which seeks to determine the minimum number of guards required to monitor an art gallery with  $n$  walls. The area that can be seen from a specific point forms what is known as a *visibility polygon* [6].

On the other hand, two points  $p$  and  $q$  are defined as  $k$ -visible if the line segment connecting them intersects the exterior of polygon  $P$  no more than  $k$  times [6]. Consequently, for a given  $k$ , it is possible to determine the  $k$ -visible region from a particular vantage point  $p$ .

Fig. 1 shows a map displaying various  $k$ -visibility values from the viewpoint of a point marked in dark blue within the red area. Here, red cells indicate 0-visibility, green cells represent 1-visibility, blue cells correspond to 2-visibility, and yellow cells denote 3-visibility.

The vantage point  $p$  is referred to as a  $k$ -transmitter, and  $k$ -visible polygons can be identified for each value in the set  $\{0, 1, \dots, k\}$  [6]. Several algorithms exist to generate  $k$ -visibility plots, each with varying levels of computational complexity [49]–[51].

### IV. DENSE INVERSE $k$ -VISIBILITY

In this section, we will go over the preliminaries and concept of the proposed *dense inverse  $k$ -visibility*, starting with an overview of the algorithm involved, with focus in the next section its application in robotics.

$k$ -visibility deals with the numeric assignment of a region of space, based on the visibility of that space in reference to some known  $k$ -router or  $k$ -transmitter. It is based on ray casting in various directions, with many  $k$ -visibility works casting from  $k$ -router-point to current trajectory point, with  $k$ -value dependent on whether the casted ray intersects with an obstruction or obstacle. The rule is in  $k$ -visibility, the ray is made of subparts, with different  $k$ -values at these obstructions. These points along the ray where  $k$  changes

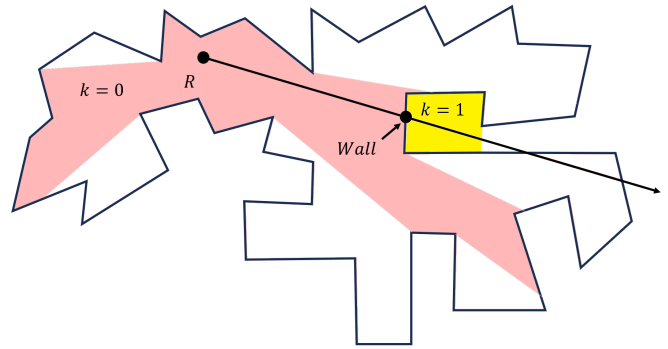


Fig. 2. Diagram illustrating the ray-drawing principle fundamental to the inverse  $k$ -visibility algorithm. The wall is located where two consecutive  $k$ -value regions intersect along a ray projected from the router point. Only the region within the  $k = 1$  area is displayed.

are namely where walls or occupied space is detected. A wall is located at the coincident point between two adjacent differing  $k$ -values.

The inverse  $k$ -visibility algorithm is based in the reverse of the  $k$ -visibility concept, where from the  $k$ -value regions, instead of using the environment map as input, these  $k$ -value regions help to provide the map as output instead. This algorithm does so by doing ray-casting and deeming the changes between  $k$ -values as a wall location or occupied space. Fig. 2 demonstrates this ray drawing principle.

In this regard, if the entire set of points representing the change in  $k$ -values is found, then the full information of the environment map can be extracted by this inverse  $k$ -visibility algorithm. Color-coded according to differing  $k$ -values can be done and this can be used as input code map of all superimposed  $k$ -visibility plots for all values  $k$ , with respect to a known  $k$ -router or  $k$ -transmitter reference position, where in which the entire  $k$ -visibility is based on, as in Fig. 1. It is clear that wall and occupied positions lie on the intersection between consecutive  $k_{i-1}k_i$  portions of the  $k$ -visible map. The details of the full inverse  $k$ -visibility algorithm are that it detects shared pixel spaces among successive  $k$ -value areas, superposes them on a separate image, using black-and-white outlining to generate the environment map.

### V. SPARSE INVERSE $k$ -VISIBILITY

Extracting the  $k$ -value for the entire environment plot can often be too computationally demanding and renders the full approach not feasible. An alternative is to only do a subpart of the map, extracting instead *sparse  $k$ -values*, this approach wherein here we call *sparse inverse  $k$ -visibility* is based on relating coordinates of known consecutive  $k$ -value coordinates located along the same casted ray from the router point to the trajectory. An estimate can be made of the router position and trajectory by dead reckoning using inertial measurement units or wheel encoders, whichever of the two is available for use in odometry.

We now go over the algorithm in greater detail. First, assume that we are in an indoor environment whose map we are trying to determine, assume that the router position

*$k_i$  number of walls along this line*

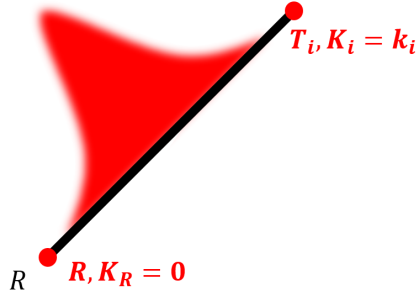


Fig. 3. Ray-drawing for an arbitrary trajectory coordinates  $T_i$  with an associated  $k$ -value  $k_i$ . According to the definition of  $k$ -visibility, the ray  $\overline{RT}_i$  must intersect exactly  $k_i$  walls along its path.

is defined and well known,  $R = (r_x, r_y)$ . Assume that a user or mobile robot, which of whom is connected to this router signal's WiFi network, is traversing the indoor space with trajectory  $T = [T_1, T_2, \dots, T_{max}]$  where  $T_i$  represents the  $(x, y)$  position of a point along the  $i^{th}$  coordinate in the trajectory. Assume that along with trajectory  $T$ , there is set  $K = [K_1, K_2, \dots, K_{max}]$  where  $K_i$  represents the associated  $k$ -value from router position  $R$  to trajectory in  $i$ -th step  $T_i$ , where  $k$  is represented here as the integer representing the number of obstacles present in the casted ray from router  $R$  to trajectory in this  $i$ -th step  $T_i$ .

This approach is probabilistic, and so *probabilistic sparse inverse  $k$ -visibility* algorithm then works in three parts:

- 1) Extracting  $k$ -values: for each coordinate, we have an associated  $k$ -value with respect to a known router position (See Sec. V-A);
- 2) Mapping Free Space: knowing when a space is obstacle or obstruction-free is defined (See Sec. V-B);
- 3) Mapping Occupied Space: the probabilistic approach is in classifying the obstacle or obstruction space, using a three-step process which is firstly to extract the casted ray, then do ray segmentation, apply Gaussian probability defining (See Sec. V-C).

This probabilistic sparse inverse  $k$ -visibility algorithm assumes that the environment map is organized in a 2D grid format. This takes the form of occupancy grid map style of mapping. From [52], occupancy grid mapping assumes perfectly cut tiles as subparts on the map environment. To make note of, under this assumption, the map is approximated and not continuous as it truly is apart from a grid. This then also would mean we make the assumption too that our casted ray array  $\overline{RT}_i$ 's elements are elements from tiles of a grid from router to trajectory. And based off of  $k$ -visibility, this ray is bound to have a  $k_i$  number of walls defined in its array. And so, if a space is deemed occupied, walls then are approximated as taking discrete filled out tiles from this grid map environment. This concept is shown in Fig 3.

#### A. Extracting $k$ -values

A wall prediction model was proposed by Fafoutis *et al.* [53], in which  $k$ -values were set based on RSSI measurements in a real experimental scenario, based on trajectory traversed by a wearable sensor and a known access point. By this regard, the model is known to be a RSSI-based wall predictor whose function uses wearable sensor position as input to output the number of walls from this point to the known access point. This predicted number of walls has an upper bound of  $K$  based on a sequence of RSSI bounds,  $t_1, t_2, \dots, t_K$  with function form [53]:

$$f(P_{RSSI}) = \begin{cases} 0 & \text{if } P_{RSSI} > t_1 \\ 1 & \text{if } t_1 \geq P_{RSSI} > t_2 \\ \vdots & \\ K-1 & \text{if } t_{K-1} \geq P_{RSSI} > t_K \\ K & \text{if } t_K \geq P_{RSSI} \end{cases} \quad (1)$$

To note, RSSI signal strength weakens when passing through an obstacle, obstruction or wall, and so the following further is assumed:

$$t_K < t_{K-1} : k \in [1, K] \quad (2)$$

We use  $K$ -Means algorithm for the sake of brevity and simplicity, as the task is based in unsupervised learning and requiring no training utilizing labelled data. This is a good approach for the purposes of Structure from Wifi mapping.

Utilizing  $K$ -Means algorithm in the context of  $K$  walls via the algorithm by Fafoutis *et al.*, the resulting output is  $K+1$  centroids, which of whom we sort as  $C_0, C_1, \dots, C_K$ . Bounds on the RSSI can then be defined as:

$$t_k = \frac{C_{k-1} + C_k}{2} : k \in [1, K] \quad (3)$$

This framework and the guiding equations define the basis of our proposed sparse inverse  $k$ -visibility algorithm. We conduct experimental trials utilizing this framework.

It is worth making note that in real-world experiments, RSSI signals oscillate greatly and exhibit much noise. To account for this noise and thus the fluctuation of the RSSI measurements in hopes to improve accuracy, we apply a slider window filter as the wearable sensor traverses its trajectory path.

#### B. Mapping Free Space

To map the free space, we employed a set of geometric rules as illustrated in Fig. 4. Initially, we assume that the pixel values of the map are unknown setting to 127. The trajectory is first segmented according to the  $k$ -values, as detailed in Sec. V-A. Subsequently, these rules are applied to identify the free space. Full details are described in Alg. 1.

**Rule 1:** The robot's trajectory is considered as free space unless it encounters an obstacle, detected by contact sensors.

**Rule 2:** If  $k = 0$ , the pixels on the line segment between the router and the robot are free space.

**Rule 3:** If  $k \geq 1$ , there are walls between the router and the robot.

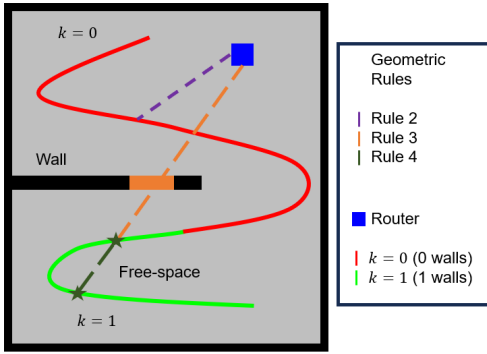


Fig. 4. Visual demonstration of the geometric rules for areas with  $k = 0$  and  $k = 1$ . Rule 1, depicting the robot's trajectory, was omitted from the legend for clarity. Figure adapted from SfW[5].

**Rule 4:** For any line emanating from a router, if the line intersects the robot trajectory at two points with the same  $k$ -values, the pixel residing on the line that is between the two points belongs to the free space.

**Rule 5:** As the  $k$ -values are determined, the confidence level of each pixel being classified as free space or a wall is updated probabilistically.

### C. Mapping Occupied Space

Segmenting the trajectory based on the  $k$ -value and continuity is the initial step in the algorithm for identifying occupied/free space. The algorithm categorizes trajectory coordinates according to their respective  $k$ -values.

To identify free space, a ray is drawn from the Router  $R$  to all trajectory coordinates with  $k$ -values equal to 0. By the definition of  $k$ -visibility, no walls obstruct these lines, thus all cells along these  $k_0$  rays are classified as free space.

Following this, the outer walls are approximated by drawing a rectangular bounding box around all data points, including trajectory coordinates and cells identified by the rays. This provides an outline of the indoor floorplan, based on the assumption that the robot navigates through all rooms within the map.

To further identify walls within the map, a probabilistic model is applied based on Geometric Rule 5. Consider the ray  $\overline{RT}_i$  depicted in Fig. 5, where the  $k$ -values for the trajectory position  $K_i = 1$ . Given the  $k$ -visibility, it is known that  $\overline{RT}_i$  intersects exactly  $K_i$  wall cells, which, in this case, is one wall cell. With no other known information, the most reasonable assumption is that this wall cell is located at the midpoint of  $\overline{RT}_i$ . The validity of this assumption decreases as the length of the ray increases. This probabilistic certainty is represented as:

$$\mu_j = \frac{e^{-\left(\frac{1}{M}\right)^2 d_j}}{L}, \quad (4)$$

where  $\mu_j$  is the probability of the  $j^{\text{th}}$  cell being a wall,  $M$  is the number of intermediate cells along the ray,  $L$  is the length of the ray, and  $d_j$  is the distance from the  $j^{\text{th}}$  cell to the ray's midpoint. Intermediate cells are defined as all cells along the ray, excluding the endpoints.

The prediction accuracy for ray  $\overline{RT}_i$  in Fig. 5 can be improved by adjusting the ray endpoints, resulting in a shorter line and fewer intermediate cells, thereby enhancing the probability estimation. Initially, the lower endpoint of a ray,  $e_{\text{lower}}$ , is the router point  $R$ , and the upper endpoint,  $e_{\text{upper}}$ , is the trajectory point  $T_i$ . If the ray intersects other trajectory points, these points serve as updated endpoints. The lower endpoint is updated if the intersecting trajectory point  $T_j$  has  $K_j = 0$ ; otherwise, the upper endpoint is updated if  $K_j \geq 1$ .

The approach can be extended to handle cases where  $k$ -values is greater than 1. For each trajectory coordinate, a ray  $\overline{RT}_i$  is drawn, and trajectory intersections are identified as previously described. The ray is then segmented based on these trajectory intersections. The difference  $\Delta k$  between the endpoints of each subsegment is calculated, as shown in Fig. 6. If  $\Delta k = 0$ , meaning that the endpoints have the same  $k$ -value, the segment is considered as free space. If  $\Delta k = 1$ , indicating that exactly one wall lies along the subsegment, an unimodal probability distribution is applied, with the highest probability at the midpoint, assuming no additional information is available. For  $\Delta k > 1$ , multiple walls are along the subsegment and a multimodal distribution is applied.

When rays are drawn for each cell along the trajectory, it's possible for a cell to be "seen" from multiple rays. In such cases, the cell would already have an assigned probability from a previous ray, as calculated by Eq. (4). The probability for the cell is then updated by integrating the probabilities from both the prio and current rays, weighted by their respective uncertainties.

$$\mu = \frac{\sigma_1^2}{\sigma_1^2 + \sigma_2^2} \mu_2 + \frac{\sigma_2^2}{\sigma_1^2 + \sigma_2^2} \mu_1 \quad (5)$$

Here,  $\mu$  represents the combined probability,  $\mu_1$  and  $\mu_2$  are the probabilities assigned by the previous and current rays, respectively, and  $\sigma_1$  and  $\sigma_2$  are the associated uncertainties of these probabilities. These procedures are outlined in Alg. 1. Initially, the robot's position  $(x, y)$  is set within its trajectory  $T$  (ln 1). The map  $M$ , which is initialized to a pixel value of 127 (unknown space, corresponding to a probability of occupancy of 0.5) (ln 2). The positions of  $n$  routers are defined within the map and the focused router position is initially set to the first router by default (ln 3-4). As the robot

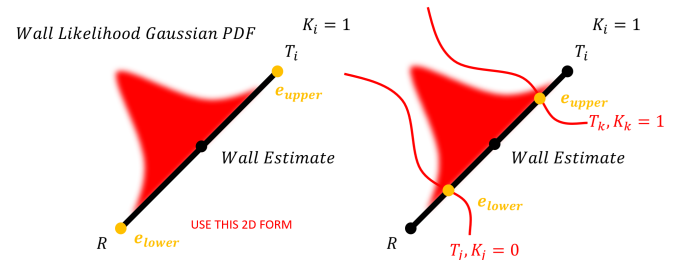


Fig. 5. Initial wall estimate along a ray (left). Enhanced wall estimation along a ray after adjustments to the lower and upper endpoints (right).

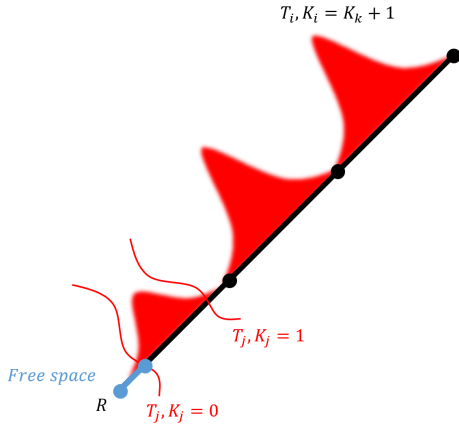


Fig. 6. Assigning probability distributions based on the variations in  $k$ -values across ray subsegments.

moves to the next trajectory coordinates  $(x_j, y_j)$ , it marks the current position  $(x_i, y_i)$  as free space on the map with a pixel value of 255 (Rule 1, corresponding to a probability of occupancy of 1) (ln 5). For each router  $(a_k, b_k)$ , the algorithm calculates the RSSI value  $R_k$  from the current position  $(x_i, y_i)$  to the router (lns 6-7). If the RSSI value  $R_k$  from a new router is stronger than the previous one, the focused router position is updated to  $(a_k, b_k)$  (lns 8-10). The algorithm iterates through all points from the robot's position  $(x_i, y_i)$  to the focused router position  $(a_k, b_k)$  (ln 11). For each point  $(t_x, t_y)$ , it computes the  $k$ -value based on a probabilistic model following the geometric rules from Sec. V-B (lns 12-14). If  $K_i = 0$ , the probability of walls is increased by  $\sigma$  (Rule 2) closer to a pixel value of 255, and if  $K_i \geq 1$ , the probability of free space is reduced by  $\sigma$  (Rule 3) closer to a pixel value of 0 (lns 15-19). If the distance  $(d(c, d))$  is such that the  $k$ -value at point  $c$  and  $d$  ( $K_c = K_d$ ), all points along the Line between two points increase the probability being free space by  $\sigma$  (lns 20-24). Throughout this process, the map is continuously updated with the RSSI values, constructing the environment map (lns 25-28).

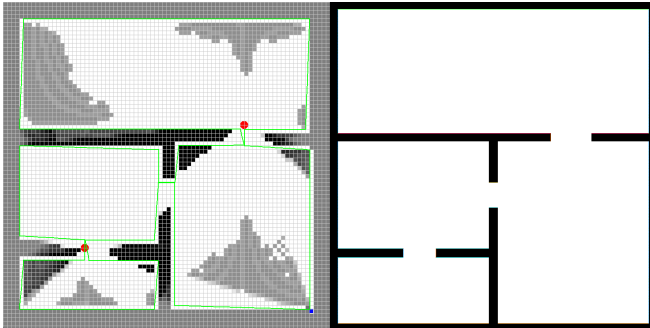


Fig. 7. Simulated results utilizing the proposed algorithm. (left): Displays free space and occupied cells, with the robot's trajectory depicted in green. (right): Shows the Ground-truth map [54]. Figure adapted from prior SFW[5].

### Algorithm 1 Multi-Router Free Space Mapping

- 1: **initialize:** Robot position  $(x, y) \in T$ ,
- 2: trajectory  $T \in M$ , map  $M_{ij} \in \{\mathbb{R}^2\} \forall i, j, M_{ij} \leftarrow 127$ ,
- 3: and  $n$  router positions  $(a_1, b_1), (a_2, b_2), \dots, (a_n, b_n) \in M$ . Set focused router position as  $(a, b) = (a_1, b_1) \in M$ .
- 4: **while** Robot goes to next position  $(x, y)_i \leftarrow (x, y)_{i+1}$  **do**
- 5: Set  $M_{(x, y)_i} \leftarrow 0$  (free space) [Rule 1].
- 6: **for all**  $(a_k, b_k) \in \{(a_1, b_1), (a_2, b_2), \dots, (a_n, b_n)\}$  **do**
- 7:  $R_k \leftarrow P_{RSSI}$  from  $(t_x, t_y)$  to  $(a_k, b_k)$ ,  $R_i \in \mathbb{R}$ .
- 8: **if**  $R_{k-1} < R_k$  and  $k > 1$  **then**
- 9: Set focused router position as  $(a, b) = (a_k, b_k)$ .
- 10: **end if**
- 11: **end for**
- 12: **for all**  $(t_x, t_y) \in M$  from  $(x, y)$  to  $(a, b)$  **do**
- 13:  $L_i \leftarrow P_{RSSI}$  from  $(t_x, t_y)$ ,  $L_i, P_{RSSI} \in \mathbb{R}$ .
- 14:  $K_i \leftarrow f(P_{RSSI})$  from  $(t_x, t_y)$ ,  $K_i \in \mathbb{R}$ .
- 15: **if**  $K_i = 0$ , **then**
- 16:  $L_i = L_i + \sigma$  (increase prob. free space) [Rule 2].
- 17: **else if**  $K_i \geq 1$ , **then**
- 18:  $L_i = L_i - \sigma$  (increase prob. of walls) [Rule 3].
- 19: **end if**
- 20: **if**  $\exists c, d \in \mathbb{R}$  such that  $K_c = K_d$ , **then**
- 21: **for all**  $L_i$  from  $L_c$  to  $L_d$  **do**
- 22:  $L_i = L_i + \sigma$  (increase prob. free space)
- 23: [Rule 4].
- 24: **end for**
- 25: **end if**
- 26: Update map  $M$  by  $P_{RSSI}$  of  $(t_x, t_y) \leftarrow L_i$ .
- 27: **end for**
- 28: **end while**

## VI. EXPERIMENTAL RESULTS

This section presents the implementation of sparse inverse  $k$ -visibility under simulated and real-world experiments to validate its robustness. We also test the improvement from single-router to multi-router cases.

In the simulated environment, as shown in Fig. 7, a robot travels along an ideal trajectory, defined as a trajectory path that follows along the walls and explores all walls of each room. This ensures detailed mapping of the environment's boundaries. The floorplan map was provided by the House-Expo dataset [54]. As the robot travels around the room, every trajectory coordinate is associated with a unique  $k$ -value based on its current and relative position to the router. From the simulated result, free space and walls are estimated with great accuracy compared to ground truth when given the optimal path.

For the real-world experiments, the lidar map using a 360 Laser Distance sensor (LDS-01) was used as ground-truth data to validate our algorithms on 2D occupancy grid map. Our algorithm is heavily dependent on the optimality and quality of the robot trajectory to estimate the map. The odometry data from the TurtleBot3 was used for the  $(x, y)$

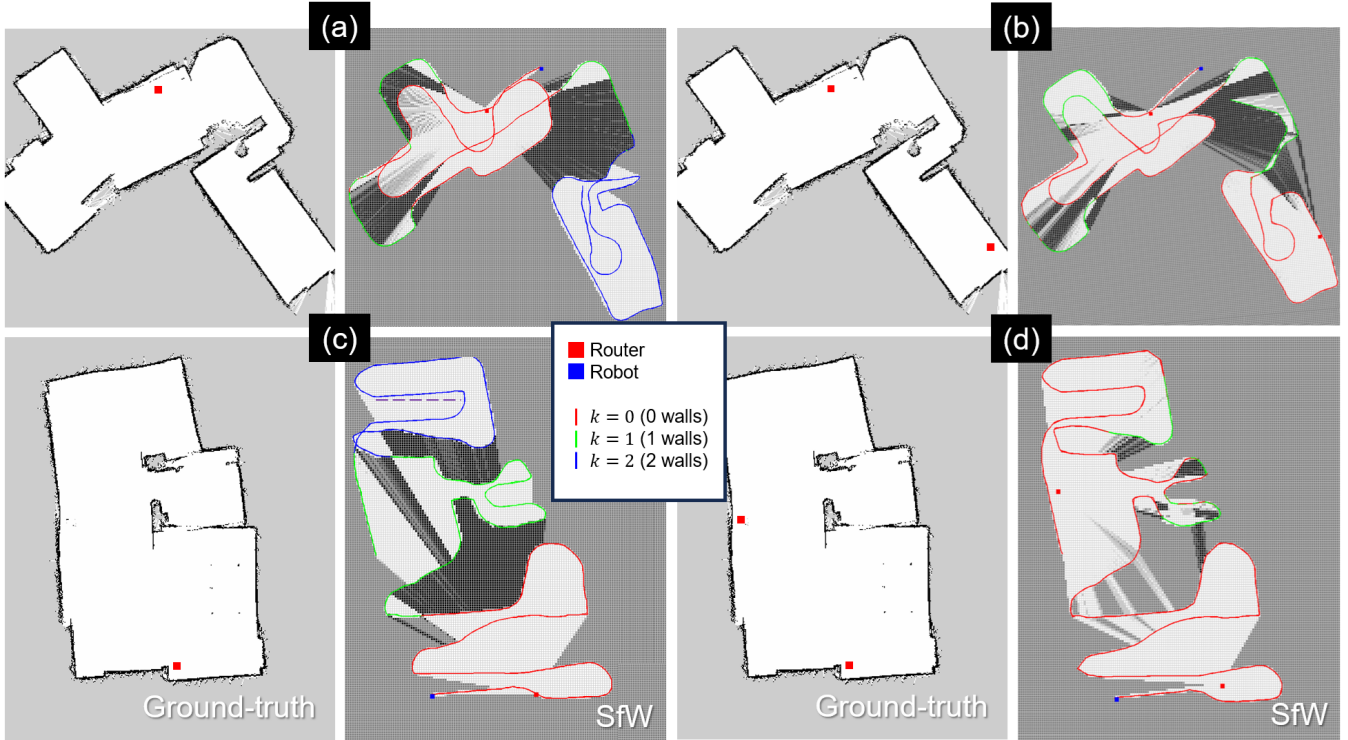


Fig. 8. Real-world experimental results for single-router and multi-router SfW mapping. (a) and (b) are for the same environment, but with one and two routers respectively. The same applies to (c) and (d). Our proposed method with RSSI-based mapping detects most of the free space and potential walls with  $k \geq 1$ . The multi-router case has improved accuracy in estimating its map.

coordinate of the robot at all points along the trajectory, and RSSI signal strengths were measured at each position. A total of four different trajectories were tested under different environments, including some challenging environments with complex floor plans. In all cases, we assumed that the router’s location is known; however, even if the location is unknown, it can be easily estimated using other algorithms and signal strength. Robot trajectory was set to explore all walls within the floor plan.

#### A. Evaluation Metrics

Prior to any metric evaluation, the RSSI-generated map must be aligned and superposed along the ground-truth lidar map, both discretized by an aligned occupancy grid map. Each grid element on the grid map represents a small-element subset of the entire  $M \times N$  map which is used for element-wise comparison. Here, we will present the evaluation metrics used in measuring the experimental accuracy after alignment.

**k-value accuracy Percentage:** We use the wall prediction model proposed by Fafoutis *et al.* [53], as discussed further in Sec. V-A to obtain the  $k$ -values from the acquired RSSI values which uses a  $K$ -Means approach. The RSSI-generated map is then estimated by Alg. 1. From the ground-truth map, we then construct expected  $k$ -values based on the positioning of the routers and the wall obstacles.

Ultimately, the  $k\text{-value}_{accuracy}$  is an element-by-element comparison of the estimate  $k$ -values from the estimate RSSI-generated map and the ground-truth  $k$ -values from the

ground-truth map. If the estimate  $k$ -value is the same as the expected on the ground truth, it is deemed predicted True and,

$$k\text{-value}_{True} = k\text{-value}_{True} + 1, \quad (6)$$

with no change if the prediction is not correct, deemed predicted False. After all  $M \times N$  elements, the  $k$ -value accuracy is calculated by,

$$k\text{-value}_{accuracy} = \frac{k\text{-value}_{True}}{M \times N} \times 100\%. \quad (7)$$

**IOU Score:** A mask  $Z$  on each coordinate  $(i, j) \in M \times N$  first needs to be applied on the RSSI-estimate  $RSSI E$  map to exclude any estimates that are neither considered free-space or a wall:

$$Z(i, j) = \begin{cases} 1 & \text{if } RSSIE(i, j) \neq 127 \\ & \text{and } GT(i, j) \neq 127 \\ 0 & \text{otherwise} \end{cases} \quad (8)$$

where  $GT$  is ground-truth map of  $M \times N$ . Then, the mask  $Z$  is applied to filter out the uncertain parts by an intersection,

$$I(i, j) = \begin{cases} 1 & \text{if } RSSIE(i, j) \neq 0 \\ & \text{and } GT(i, j) \neq 0 \\ & \text{and } Z(i, j) = 1 \\ 0 & \text{otherwise} \end{cases} \quad (9)$$

Next, account for the entire map by a union  $U$  where the element is certain (either free-space or wall),

$$U(i, j) = \begin{cases} 1 & \text{if } (RSSIE(i, j) \neq 0 \\ & \text{or } GT(i, j) \neq 0 \\ & \text{and } Z(i, j) = 1 \\ 0 & \text{otherwise} \end{cases} \quad (10)$$

The IOU Score  $IOU_{score}$  is then calculated by,

$$IOU_{score} = \frac{\sum_{i,j} I(i, j)}{\sum_{i,j} U(i, j)} \quad (11)$$

**MSE Score:** First, the difference  $D_{i,j}$  is taken element-wise between  $RSSIE$  and  $GT$  and then squared  $DS$ ,

$$D(i, j) = RSSIE(i, j) - GT(i, j) \quad (12)$$

$$DS(i, j) = (D(i, j))^2 = (RSSIE(i, j) - GT(i, j))^2 \quad (13)$$

Next, MSE Score  $MSE_{score}$  is the mean of the square differences  $DS$ , and is calculated by,

$$\begin{aligned} MSE_{score} &= \frac{1}{N \times M} \sum_{i,j} DS(i, j) \\ &= \frac{1}{N \times M} \sum_{i,j} (RSSIE(i, j) - GT(i, j))^2 \end{aligned} \quad (14)$$

Note, the unit of MSE Score is in Square Pixel ( $px^2$ ).

## B. Quantitative Results

Experiments 1 and 2 from SfW[5] results are extended for the single-router case to include comparison by mapping area, number of data points,  $k$ -value prediction True/False setting,  $k$ -value accuracy percentage, IOU and MSE scores. Further analysis was conducted to evaluate our proposed method, as shown in Table. I. Experiments 5-6 show improved performance with fewer data points. This is because their experiments utilize two routers instead of one. With two routers, more data is collected simultaneously, and the most optimized data is selected from various cases. In contrast, using a single router provides only one piece of information at a time causing less efficient data collection.

In the first experiment, a total of 3159 data points were collected and showed 84.93%  $k$ -value prediction accuracy. Here, the Intersection Over Union (IOU) score was calculated at 0.8531 comparing each corresponding pixel from the ground truth and the RSSI-generated map. The Mean Squared Error (MSE) score was 1.7770  $px^2$  showing high similarity with the ground truth.

Similarly, the second experiment showed 82.79% accuracy rate out of 4713 data points. The area of the map was more than twice of the first experiment. The IOU score and the MSE score was 0.9028  $px^2$  and 17.4238  $px^2$  respectively. Further analysis for the first and second experiments can be found in the prior SfW paper [5].

TABLE I

ACCURACY AND MAP SIMILARITY COMPARISON BETWEEN LIDAR (GROUND TRUTH) AND RSSI GENERATED MAP. FOR BREVITY,  $\uparrow$  MEANS A RESULT THAT IS LARGER IS BETTER, AND  $\downarrow$  MEANS A RESULT THAT IS LOWER IS BETTER.

	Exp.1	Exp.2	Exp.3	Exp.4	Exp.5	Exp.6
Area of Map	15.7 m <sup>2</sup>	34.2 m <sup>2</sup>	42.5 m <sup>2</sup>	51.5 m <sup>2</sup>	42.5 m <sup>2</sup>	51.5 m <sup>2</sup>
#Router	1	1	1	1	2	2
#Data points	3159	4713	6001	1803	492	393
$k$ -value Prediction True	2683	3902	5120	1698	471	379
$k$ -value Prediction False	476	811	881	105	21	14
$k$ -value Accuracy % $\uparrow$	84.93	82.79	85.32	94.18	95.73	96.44
IOU Score $\uparrow$	0.8531	0.9028	0.8321	0.9349	0.8364	0.9627
MSE Score $\downarrow$	1.7770	17.4238	9.0783	12.1403	1.6163	13.5331

## C. Single-Router to Multi-Router Evaluations

Experiments 3-6 test the proposed algorithm for multi-router cases, where it is expected that additional router sensors would greatly improve the accuracy of the map as the WiFi signal strength is superposed and strengthened. We will start with details on single-router, then, introduce more.

Starting with the single-router case, the third experiment in Fig. 8-(a) covered a trajectory dealing with 6001 data points in an area of 42.5  $m^2$  and showcased high  $k$ -value accuracy of 85.32%. In this experiment, we placed the router in a room with higher-density walls and corridors, and our algorithm can still maintain high robustness in its map. The large black spaces in our generated RSSI-based map, which are considered wall space, were, in fact, these higher-density walls showcasing the accuracy of our method. Due to the properties of our algorithm, large black spaces can be further classified as either free space of a wall with more trajectory data and RSSI data as the robot travels in that specific area.

With the multi-router case for the fifth experiment in Fig. 8-(b), the  $k$ -value accuracy greatly improves going from 85.32% to 95.73% with significantly fewer data points. The second router is leveraged in the  $k$  region where prior single-router cases struggled. As our algorithm makes each router to only prioritize the closest and strongest signal, the  $k = 0$  regime is effectively identified with minor false prediction. Details on the multi-router case for the third experiment are stated as Exp. 5 in Table I.

Next, with the single-router case for the fourth experiment in Fig. 8-(c) dealing with a map area of 51.5  $m^2$  was the largest map area space covered out of all four experiments. This case was unique where the router was placed in one end to eliminate any effects that the distance-loss might have caused. As expected, as  $k$  increases, the accuracy of our RSSI-based method might deter. This is certain for conventional mapping methods as well. As shown, for  $k = 0$ , the space generated by the RSSI-based approach is close to ground truth. As the trajectory moves in the  $k = 1$  space, the map generated is still highly accurate with two large black regions representing very well the wall spaces in our



ground-truth map. Going to  $k = 2$ , the expected free space is mapped. This experiment shows that in large area spaces where the router is not in close proximity to the robot but instead very far, our RSSI-based approach still maintains robustness in mapping, here with an accuracy of 94.18% to the real map.

With the multi-router case for the sixth experiment in Fig 8-(d), again, the RSSI map accuracy improves, this time going from 94.18% to 96.44%. The increased improvement is not as great as the third experiment, only with a 2% increase but this is due to the larger area of the fourth experiment. In comparing the single-router with the multi-router case, it is clear that in regions where the single-router map estimate fails, the multi-router tracks more accurately the free space area, whilst circumventing the false positives of walls. Exp. 6 accurately differentiates the free space/potential walls which were poorly detected in the  $k = 2$  region from the fourth experiment. Details on the multi-router case for the third experiment are stated as Exp. 6 in Table I.

#### D. Experimental Discussion Between Trajectories

While RSSI data points ranging between 393 to 6001 were collected from four experiments, all experiments have shown good estimates of the  $k$  values above 82%. In all four experiments, the algorithm shows a robust prediction capability of the RSSI signals across various environments in its high  $k$ -value accuracy percentage, its near 1 IOU score, and its relatively low MSE score, shown in Table I.

The  $k$ -value accuracy percentage was optimized higher in experiments 4-6 in larger map areas compared to the prior experiments, by the positioning of the routers and the careful traversing of the robot trajectory to optimize RSSI signal strength from the routers. This implies that methodically planning the trajectory beforehand in the map estimate is essential.

Next, the IOU score, which measures the overlap between predicted free space and the ground truth, showed little variability for all experiments ranging from 0.8-0.96, where a near 1 IOU Score indicates a good overlap between the ground truth and our algorithms.

Though the  $k$  - *value* accuracy percentage and IOU score showed great accuracy and robustness in the map estimate over all experiments, the MSE score had significant variability. Exp. 2-4 and 6 shown in Table I had larger MSE scores, but given the large area spaces, these MSE scores are within reason and alleviated when going from single-router to multi-router cases, as shown by the significant drop in MSE score of single-router Exp. 3 with MSE score of  $9.0783 px^2$  to multi-router Exp. 5 with MSE score of  $1.6163 px^2$ .

#### FUTURE WORK AND CONCLUSIONS

This paper presents an innovative approach to Wifi-based geometric mapping, which effectively estimates the approximate layout of indoor spaces, especially the free space. These free spaces are necessary for the robot to plan paths and explore unfamiliar environments. Notably, our method does not depend on crowdsourcing or exteroceptive sensors such

as a camera, radar, or lidar. Further, Our results demonstrate an overall increase in mapping accuracy by approximately 6.34% on average with about 85% fewer data points required, compared to using a single router setup.

As for future work, it will be necessary to investigate machine learning techniques to enhance the quality of the maps during post-processing. Combining WiFi-based localization for precise trajectory tracking with our WiFi-based mapping will provide a more comprehensive autonomous WiFiSLAM system. Additionally, strategies for active trajectory planning to improve map accuracy will be explored. Further research should also focus on developing advanced filtering systems that account for distance in the case of the large-scale map. Due to the characteristics of the RSSI signal, multiple routers should be incorporated for a large-scale environment. Strategic router placement is also needed for optimizing signal strength distribution and improving data quality. Routers should be positioned with minimal signal overlap and reduce areas of weak or no coverage. In most cases, this can be achieved by placing the routers at key locations such as the corners and central points of large rooms, while ensuring line-of-sight from any points.

#### ACKNOWLEDGEMENTS

We would like to thank Jill Aghyourli Zalat for her early work formulating the SfW concepts and Ishaan Mehta for his feedback and assistance with data acquisition. This research is supported by Natural Sciences and Engineering Research Council of Canada (NSERC).

#### REFERENCES

- [1] T. Kudo and J. Miura, "Utilizing WiFi signals for improving SLAM and person localization," in *2017 IEEE/SICE International Symposium on System Integration (SII)*. IEEE, 2017, pp. 487–493.
- [2] B. Ferris, D. Fox, and N. D. Lawrence, "WiFi-SLAM Using Gaussian Process Latent Variable Models," in *IJCAI*, vol. 7, no. 1, 2007, pp. 2480–2485.
- [3] B. Zhou, W. Ma, Q. Li, N. El-Sheimy, Q. Mao, Y. Li, F. Gu, L. Huang, and J. Zhu, "Crowdsourcing-based indoor mapping using smartphones: A survey," *ISPRS Journal of Photogrammetry and Remote Sensing*, vol. 177, pp. 131–146, 2021.
- [4] A. Arun, R. Ayyalasomayajula, W. Hunter, and D. Bharadia, "P2SLAM: Bearing based WiFi SLAM for Indoor Robots."
- [5] J. Kim, J. A. Zalat, Y. Bahoo, and S. Saedi, "Structure from wifi (sfw): Rssi-based geometric mapping of indoor environments," *arXiv preprint arXiv:2403.02235*, 2024.
- [6] J. O'Rourke *et al.*, *Art gallery theorems and algorithms*. Oxford University Press Oxford, 1987, vol. 57.
- [7] H. Xiong and D. Tao, "A diversified generative latent variable model for wifi-slam," in *Proceedings of the AAAI Conference on Artificial Intelligence*, vol. 31, no. 1, 2017.
- [8] R. Miyagusuku, A. Yamashita, and H. Asama, "Improving gaussian processes based mapping of wireless signals using path loss models," in *2016 IEEE/RSJ International Conference on Intelligent Robots and Systems (IROS)*. IEEE, 2016, pp. 4610–4615.
- [9] J. Huang, D. Millman, M. Quigley, D. Stavens, S. Thrun, and A. Agarwal, "Efficient, generalized indoor WiFi GraphSLAM," in *2011 IEEE international conference on robotics and automation*. IEEE, 2011, pp. 1038–1043.
- [10] R. Liu, S. H. Marakkalage, M. Padmal, T. Shaganan, C. Yuen, Y. L. Guan, and U.-X. Tan, "Collaborative SLAM based on WiFi fingerprint similarity and motion information," *IEEE Internet of Things Journal*, vol. 7, no. 3, pp. 1826–1840, 2019.
- [11] F. Herranz, A. Llamazares, E. Molinos, M. Ocaña, and M. Sotelo, "WiFi SLAM algorithms: An experimental comparison," *Robotica*, vol. 34, no. 4, p. 837, 2016.

- [12] S. He and S.-H. G. Chan, "Wi-Fi Fingerprint-Based Indoor Positioning: Recent Advances and Comparisons," *IEEE Communications Surveys & Tutorials*, vol. 18, no. 1, pp. 466–490, 2015.
- [13] V. Bellavista-Parent, J. Torres-Sospedra, and A. Perez-Navarro, "New trends in indoor positioning based on wifi and machine learning: A systematic review," in *2021 International Conference on Indoor Positioning and Indoor Navigation (IPIN)*. IEEE, 2021, pp. 1–8.
- [14] F. Liu, J. Liu, Y. Yin, W. Wang, D. Hu, P. Chen, and Q. Niu, "Survey on wifi-based indoor positioning techniques," *IET communications*, vol. 14, no. 9, pp. 1372–1383, 2020.
- [15] H. Zou, C.-L. Chen, M. Li, J. Yang, Y. Zhou, L. Xie, and C. J. Spanos, "Adversarial learning-enabled automatic wifi indoor radio map construction and adaptation with mobile robot," *IEEE Internet of Things Journal*, vol. 7, no. 8, pp. 6946–6954, 2020.
- [16] R. Ayyalasomayajula, A. Arun, C. Wu, S. Sharma, A. R. Sethi, D. Vasisht, and D. Bharadia, "Deep learning based wireless localization for indoor navigation," in *Proceedings of the 26th Annual International Conference on Mobile Computing and Networking*, 2020, pp. 1–14.
- [17] Z. Xu, B. Huang, B. Jia, W. Li, and H. Lu, "A boundary aware wifi localization scheme based on umap and knn," *IEEE Communications Letters*, vol. 26, no. 8, pp. 1789–1793, 2022.
- [18] I. Karmanov, F. G. Zanjani, I. Kadampot, S. Merlin, and D. Dijkman, "Wicluster: Passive indoor 2d/3d positioning using wifi without precise labels," in *2021 IEEE Global Communications Conference (GLOBECOM)*. IEEE, 2021, pp. 1–7.
- [19] X. Chen, H. Li, C. Zhou, X. Liu, D. Wu, and G. Dudek, "Fidora: Robust wifi-based indoor localization via unsupervised domain adaptation," *IEEE Internet of Things Journal*, vol. 9, no. 12, pp. 9872–9888, 2022.
- [20] L. Zhang, Z. Chen, W. Cui, B. Li, C. Chen, Z. Cao, and K. Gao, "Wifi-based indoor robot positioning using deep fuzzy forests," *IEEE Internet of Things Journal*, vol. 7, no. 11, pp. 10773–10781, 2020.
- [21] S. L. Ayinla, A. Abd Aziz, and M. Driberg, "Salloc: An accurate target localization in wifi-enabled indoor environments via sae-almst," *IEEE Access*, 2024.
- [22] X. Wang, Z. Yu, S. Mao, J. Zhang, S. C. Periaswamy, and J. Patton, "Maploc: Lstm-based location estimation using uncertainty radio maps," *IEEE Internet of Things Journal*, 2023.
- [23] K. Park, G. Lee, Y. Lee, D. Yoon, S. Seo, J. Yoo, and M. J. Kim, "Study on wifi-based indoor positioning prediction using machine learning techniques," in *2023 14th International Conference on Information and Communication Technology Convergence (ICTC)*. IEEE, 2023, pp. 1471–1474.
- [24] Z. Turgut and A. G. Kakisim, "An explainable hybrid deep learning architecture for wifi-based indoor localization in internet of things environment," *Future Generation Computer Systems*, vol. 151, pp. 196–213, 2024.
- [25] C. Luo, H. Hong, and M. C. Chan, "PiLoc: A self-calibrating participatory indoor localization system," in *International Symposium on Information Processing in Sensor Networks*, pp. 143–153.
- [26] H. Shin, Y. Chon, and H. Cha, "Unsupervised construction of an indoor floor plan using a smartphone," *IEEE Transactions on Systems, Man, and Cybernetics, Part C (Applications and Reviews)*, vol. 42, no. 6, pp. 889–898, 2011.
- [27] B. Zhou, Q. Li, Q. Mao, W. Tu, X. Zhang, and L. Chen, "ALIMC: Activity landmark-based indoor mapping via crowdsourcing," *IEEE Transactions on Intelligent Transportation Systems*, vol. 16, no. 5, pp. 2774–2785, 2015.
- [28] B. Zhou, Q. Li, G. Zhai, Q. Mao, J. Yang, W. Tu, W. Xue, and L. Chen, "A graph optimization-based indoor map construction method via crowdsourcing," *IEEE Access*, vol. 6, pp. 33 692–33 701, 2018.
- [29] "Walkie-Markie: Indoor pathway mapping made easy, author=Shen, Guobin and Chen, Zhuo and Zhang, Peichao and Moscibroda, Thomas and Zhang, Yongguang," in *Symposium on Networked Systems Design and Implementation*, 2013, pp. 85–98.
- [30] Y. Jiang, Y. Xiang, X. Pan, K. Li, Q. Lv, R. P. Dick, L. Shang, and M. Hannigan, "Hallway based automatic indoor floorplan construction using room fingerprints," in *ACM international joint conference on Pervasive and ubiquitous computing*, 2013, pp. 315–324.
- [31] Alzantot, Moustafa and Youssef, Moustafa, "CrowdInside: automatic construction of indoor floorplans," in *Proceedings of the 20th International Conference on Advances in Geographic Information Systems*, 2012, pp. 99–108.
- [32] J. Liang, Y. He, and Y. Liu, "SenseWit: Pervasive floorplan generation based on only inertial sensing," in *International Conference on Distributed Computing in Sensor Systems*. IEEE, 2016, pp. 1–8.
- [33] A. Gonzalez-Ruiz and Y. Mostofi, "Cooperative robotic structure mapping using wireless measurements—A comparison of random and coordinated sampling patterns," *IEEE Sensors Journal*, vol. 13, no. 7, pp. 2571–2580, 2013.
- [34] T. Deissler and J. Thielecke, "UWB-SLAM with Rao-Blackwellized Monte Carlo data association," in *2010 International Conference on Indoor Positioning and Indoor Navigation*. IEEE, 2010, pp. 1–5.
- [35] T. Deißler, M. Janson, R. Zetik, and J. Thielecke, "Infrastructureless indoor mapping using a mobile antenna array," in *International Conference on Systems, Signals and Image Processing*. IEEE, 2012, pp. 36–39.
- [36] X. Tong, H. Wang, X. Liu, and W. Qu, "Mapfi: Autonomous mapping of wi-fi infrastructure for indoor localization," *IEEE transactions on mobile computing*, vol. 22, no. 3, pp. 1566–1580, 2021.
- [37] D. B. Ninh, J. He, V. T. Trung, and D. P. Huy, "An effective random statistical method for indoor positioning system using wifi fingerprinting," *Future Generation Computer Systems*, vol. 109, pp. 238–248, 2020.
- [38] F. Shi, W. Li, C. Tang, Y. Fang, P. V. Brennan, and K. Chetty, "Decimeter-level indoor localization using wifi round-trip phase and factor graph optimization," *IEEE Journal on Selected Areas in Communications*, 2023.
- [39] R. Estrada, I. Valeriano, X. Aizaga, L. Vargas, N. Vera, and D. Zambrano, "Wifi indoor positioning system based on openwrt," in *IEEE EUROCON 2023-20th International Conference on Smart Technologies*. IEEE, 2023, pp. 728–733.
- [40] Y. Tao, L. Zhao *et al.*, "An extreme value based algorithm for improving the accuracy of wifi localization," *Ad Hoc Networks*, vol. 143, p. 103131, 2023.
- [41] B. Suleiman, A. Anaissi, Y. Xiao, W. Yaqub, A. S. Raju, and W. Alyassine, "Supervised learning-based indoor positioning system using wifi fingerprints," in *International Conference on Advances in Computing Research*. Springer, 2023, pp. 56–71.
- [42] M. H. Azaddel, M. A. Nourian, K. ShahHosseini, S. A. Junoh, and A. Akbari, "Spotter: A novel asynchronous and independent wifi and ble fusion method based on particle filter for indoor positioning," *Internet of Things*, vol. 24, p. 100967, 2023.
- [43] Y. Tao, B. Huang, L. Zhao, W. Wang *et al.*, "Cbwf: A lightweight circular boundary based wifi fingerprinting localization system," *IEEE Internet of Things Journal*, 2023.
- [44] C. Tang, W. Sun, X. Zhang, J. Zheng, J. Sun, and C. Liu, "A sequential-multi-decision scheme for wifi localization using vision-based refinement," *IEEE Transactions on Mobile Computing*, 2023.
- [45] R. Jurdi, H. Chen, Y. Zhu, B. L. Ng, N. Dawar, C. Zhang, and J. K.-H. Han, "Wherearthou: A wifi-rtt-based indoor positioning system," *IEEE Access*, vol. 12, pp. 41 084–41 101, 2024.
- [46] R. Fabila-Monroy, A. R. Vargas, and J. Urrutia, "On modem illumination problems," *XIII encuentros de geometria computacional, Zaragoza, Spain*, 2009.
- [47] O. Aichholzer, R. Fabila-Monroy, D. Flores-Penalzo, T. Hackl, C. Huemer, J. Urrutia, and B. Vogtenhuber, "Modem illumination of monotone polygons," in *25th European Workshop on Computational Geometry*, 2009, p. 167.
- [48] V. Klee, "Is every polygonal region illuminable from some point?" *The American Mathematical Monthly*, vol. 76, no. 2, pp. 180–180, 1969.
- [49] A. L. Bajuelos, S. Canales, G. Hernández-Penalver, and A. M. Martins, "A Hybrid Metaheuristic Strategy for Covering with Wireless Devices," *J. UCS*, vol. 18, no. 14, pp. 1906–1932, 2012.
- [50] Y. Bahoo, P. Bose, S. Durocher, and T. C. Shermer, "Computing the k-Visibility Region of a Point in a Polygon," *Theory of Computing Systems*, vol. 64, no. 7, pp. 1292–1306, 2020.
- [51] Y. Bahoo, B. Banyassady, P. K. Bose, S. Durocher, and W. Mulzer, "A time-space trade-off for computing the k-visibility region of a point in a polygon," *Theoretical Computer Science*, vol. 789, pp. 13–21, 2019.
- [52] S. Thrun, "Robotic mapping: A survey," *Exploring Artificial Intelligence in the New Millennium*, p. 1–35, 2003.
- [53] X. Fafoutis, E. Mellios, N. Twomey, T. Diethe, G. Hilton, and R. Piechocki, "An RSSI-based wall prediction model for residential floor map construction," in *World Forum on Internet of Things*. IEEE, 2015, pp. 357–362.
- [54] L. Tingguang, H. Danny, L. Chenming, Z. Delong, W. Chaoqun, and M. Q.-H. Meng, "HouseExpo: A Large-scale 2D Indoor Layout

Dataset for Learning-based Algorithms on Mobile Robots," *arXiv preprint arXiv:1903.09845*, 2019.